

Exploring the p-n junction region in Cu(In,Ga)Se₂ thin-film solar cells at the nanometer-scale

O. Cojocaru-Mirédin, P. Choi, R. Wuerz, and D. Raabe

Citation: *Appl. Phys. Lett.* **101**, 181603 (2012); doi: 10.1063/1.4764527

View online: <http://dx.doi.org/10.1063/1.4764527>

View Table of Contents: <http://apl.aip.org/resource/1/APPLAB/v101/i18>

Published by the [American Institute of Physics](#).

Related Articles

Influence of the dynamic lattice strain on the transport behavior of oxide heterojunctions

Appl. Phys. Lett. **102**, 022423 (2013)

Band offsets and heterostructures of two-dimensional semiconductors

Appl. Phys. Lett. **102**, 012111 (2013)

Energy band alignment of InGaZnO₄/Si heterojunction determined by x-ray photoelectron spectroscopy

Appl. Phys. Lett. **101**, 252111 (2012)

Response to "Comment on 'Zener tunneling semiconducting nanotubes and graphene nanoribbon p-n junctions'" [Appl. Phys. Lett. **101**, 256103 (2012)]

Appl. Phys. Lett. **101**, 256104 (2012)

Comment on "Zener tunneling in semiconducting nanotubes and graphene nanoribbon p-n junctions" [Appl. Phys. Lett. **93**, 112106 (2008)]

Appl. Phys. Lett. **101**, 256103 (2012)

Additional information on Appl. Phys. Lett.

Journal Homepage: <http://apl.aip.org/>

Journal Information: http://apl.aip.org/about/about_the_journal

Top downloads: http://apl.aip.org/features/most_downloaded

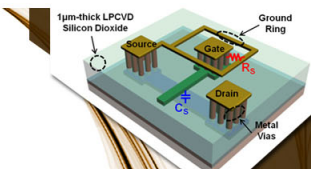
Information for Authors: <http://apl.aip.org/authors>

ADVERTISEMENT

AIP | Applied Physics
Letters


**EXPLORE WHAT'S
NEW IN APL**

SUBMIT YOUR PAPER NOW!



**SURFACES AND
INTERFACES**

Focusing on physical, chemical, biological, structural, optical, magnetic and electrical properties of surfaces and interfaces, and more...



**ENERGY CONVERSION
AND STORAGE**

Focusing on all aspects of static and dynamic energy conversion, energy storage, photovoltaics, solar fuels, batteries, capacitors, thermoelectrics, and more...

Exploring the p-n junction region in Cu(In,Ga)Se₂ thin-film solar cells at the nanometer-scale

O. Cojocaru-Mirédin,^{1,a)} P. Choi,^{1,b)} R. Wuerz,² and D. Raabe¹¹Max-Planck-Institut für Eisenforschung, Max-Planck-Straße 1, 40237 Düsseldorf, Germany²Zentrum für Sonnenenergie- und Wasserstoff-Forschung Baden-Württemberg, Stuttgart, Germany

(Received 9 July 2012; accepted 15 October 2012; published online 2 November 2012)

In this work we study the CdS/Cu(In,Ga)Se₂ p-n junction region in Cu(In,Ga)Se₂ thin-film solar cells using atom probe tomography. A Cu-, Ga-depleted, and Cd-doped region of about 1 nm thickness is detected at the Cu(In,Ga)Se₂ side of the CdS/Cu(In,Ga)Se₂ interface. Furthermore, Cd is also found to be enriched at Cu(In,Ga)Se₂ grain boundaries connected to the CdS layer. Na and O impurities decorate the CdS/CIGS interface, where Na-rich clusters are preferentially located in CdS regions abutting to Cu(In,Ga)Se₂ grain boundaries. The experimental findings of this work demonstrate the capability of atom probe tomography in studying buried interfaces and yield vital information for understanding and modeling the p-n junction band structure in Cu(In,Ga)Se₂ solar cells. © 2012 American Institute of Physics. [<http://dx.doi.org/10.1063/1.4764527>]

Thin-film solar cells based on CuInSe₂ (CIS) and Cu(In,Ga)Se₂ (CIGS) are among the most promising candidates for large-scale photovoltaic energy conversion because of their high efficiency, long-term stability, and low-cost production.^{1–3} The current record energy conversion efficiency for CIGS solar cells is 20.3%, which is the highest among all thin-film photovoltaic technologies.⁴ Despite the outstanding performance of CIGS solar cells, the exact chemical composition at the CdS/CIGS interface has remained unknown, in particular, at or below the nanometer scale. Such lack of information has impeded understanding and accurate modeling of the band structure at the p-n junction region.

The CdS/CI(G)S interface was previously investigated by energy dispersive x-ray spectroscopy (EDX),^{5–7} x-ray photoelectron spectroscopy (XPS),⁸ Auger electron spectroscopy (AES),⁸ secondary ion mass spectrometry (SIMS),⁸ and scanning Kelvin probe microscopy (SKPM).⁹ These studies showed that the buffer/absorber layer interface is intermixed. Furthermore, some of the authors measured a Cd-doped zone close to the CI(G)S surface.^{5,6} However, no accurate compositional data of these Cd-doped regions exist due to the limited spatial resolution of these techniques.

Recently, we studied the compositional gradient across the CdS/CIS interface with sub-nanometer resolution¹⁰ using laser-assisted atom probe tomography (APT).¹¹ We could clearly resolve a Cd-enriched/Cu-depleted zone of ~2 nm in thickness at the CIS surface. However, the conclusion of the previous study was that the APT results for this particular CIS solar cell cannot be generally transferred to CIGS solar cells, as different compositions and growth recipes for the absorber layers might result in different compositional gradients at the CdS/CI(G)S interface. Therefore, the current work elucidates the elemental distribution across the p-n junction region in a CIGS thin-film solar cell using APT.

Both, absorber composition (Ga is present in CIGS but not in CIS) and growth processing (multi-stage¹² instead of

single-stage growth¹³) differ substantially from the previous work.¹⁰ In contrast to the single-stage process, which only shows a slight In concentration gradient,¹³ the multi-stage grown absorber has a cup-shaped Ga profile and dome-shaped In profile typical of multi-stage grown absorbers.¹⁴ Such concentration profiles lead to bandgap grading which is favorable for charge carrier collection and the CIGS cells obtained from the current multi-stage process yield much higher energy conversion efficiency (~15%¹⁴) than the previously studied single-stage grown CIS solar cell (~9%¹⁰).

Thus, the APT data presented in this work are more representative for high-performance CIGS solar cells. In addition to the compositional gradients at the CdS/CIGS interface, we report on the distribution of impurities, namely, Na and O, at the CdS/CIGS interface. We demonstrate that APT yields vital information for modeling the p-n junction band structure in Cu(In,Ga)Se₂ solar cells.

The studied solar cell was fabricated by co-evaporation of a polycrystalline CIGS absorber film ([Cu]/([In] + [Ga]) = 0.86, [Ga]/([Ga] + [In]) = 0.28) onto a Mo-coated soda-lime glass substrate in a multi-stage inline process.¹² A CdS layer (~60 nm in thickness) was deposited on top of the CIGS film by chemical bath deposition (CBD), using a mixture of CdSO₄, ammonia, and thiourea. For simplifying the preparation of needle-shaped APT samples, the CdS layer growth was done for several times to obtain a thicker CdS layer, where no ZnO layer was deposited. Reference cells were completed with a thin CdS layer (~60 nm), a ZnO front contact layer, and an Al metal grid, which yielded a cell efficiency of 15%.

The microstructure of the CdS and CIGS film was studied by (scanning) transmission electron microscopy ((S)TEM), using a JEOL 2200 FS TEM operated at 200 kV. APT experiments were performed with a local electrode atom probe (LEAPTM 3000X HR, Cameca Instruments), applying laser pulses of 532 nm wavelength, 12 ps pulse length, and an energy of 0.1 nJ per pulse at a repetition rate of 100 kHz. The specimen base temperature was about 60 K. APT samples were prepared using a dual beam focused-ion-beam (FIB) (FEI Helios Nanolab 600) according to the procedure

^{a)}E-mail: o.cojocaru-miredin@mpie.de.^{b)}E-mail: p.choi@mpie.de.

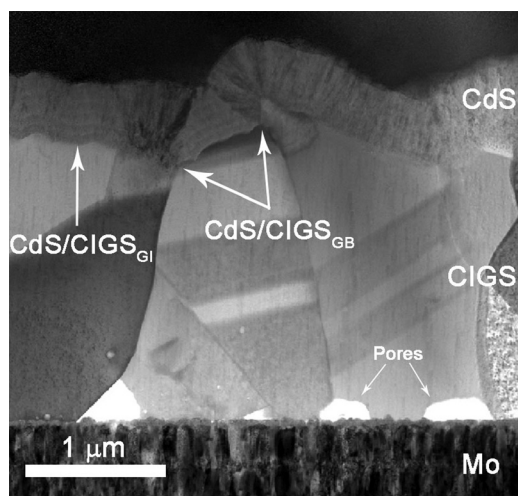


FIG. 1. Cross-sectional STEM bright-field image showing the layer stack of the studied CIGS solar cell.

described in Ref. 15. To minimize beam damage, a low energy (5 keV) Ga beam was used at the final ion-milling stage.

Fig. 1 shows the cross-sectional bright-field STEM image of the stacking CdS (400 nm)/CIGS (2 μm)/Mo (570 nm). In contrast to the polycrystalline CIGS layer (~0.5 to 2 μm in grain size, see Fig. 1), the CdS layer consists of nanometer-sized grains (~5 to 10 nm, see Fig. 2(a)). In the present work, we mark an interface region not directly abutting to a CIGS grain boundary (GB) by CdS/CIGS_{GI} and an interface region next to a CIGS GB by CdS/CIGS_{GB}, as shown in Fig. 1.

Fig. 2(a) shows a TEM image of an APT tip containing the CdS/CIGS_{GI} interface, which is oriented almost perpendicular to the tip axis (z axis). The amorphous layer formed at the tip surface during the FIB milling process at 30 keV was removed by 5 keV FIB milling before performing the APT analysis. Fig. 2(b) shows the 3D elemental maps containing the CdS/CIGS_{GI} interface and the distribution of Na and O impurities close to this interface.

Fig. 3 shows a proximity histogram (or proxigram)¹⁶ obtained from APT across the CdS/CIGS_{GI}. The interface can be defined by an iso-concentration threshold level of 7 at. % In at the intersection between the Se and S profile, as no Se or S diffusion in CdS or CIGS is expected during CBD.¹⁷ The region between -1 and +1 nm in the proxigram represents the interface region. As seen in this plot, the CdS/CIGS_{GI} interface is rather diffuse (~2 nm in width), which could be partly due to different evaporation fields of the CIGS and CdS layer and a corresponding reconstruction artefact.¹⁸

Furthermore, at the CIGS surface, there is a distinct zone of ~1 nm in width (marked in grey in Fig. 3) in which the Cu and Ga concentrations gradually decrease while the In and Se concentrations remain almost constant. In this region, a significant Cd-enrichment can be detected. The blue and orange dashed areas in Fig. 3 give the concentrations of the “missing” Cu and Ga ions, respectively, whereas the black dashed area gives the “surplus” Cd ions at the CIGS surface. From this proxigram, we could determine the concentration of “missing” Cu and Ga ions ($[\text{Cu}] + [\text{Ga}] = (9 \pm 2) \times 10^{21} \text{ cm}^{-3} + (3.5 \pm 1.5) \times 10^{21} \text{ cm}^{-3}$) and Cd “surplus” ions ($[\text{Cd}] = (1.1 \pm 0.3) \times 10^{22} \text{ cm}^{-3}$), which are nearly identical. In accordance with our previous reports on

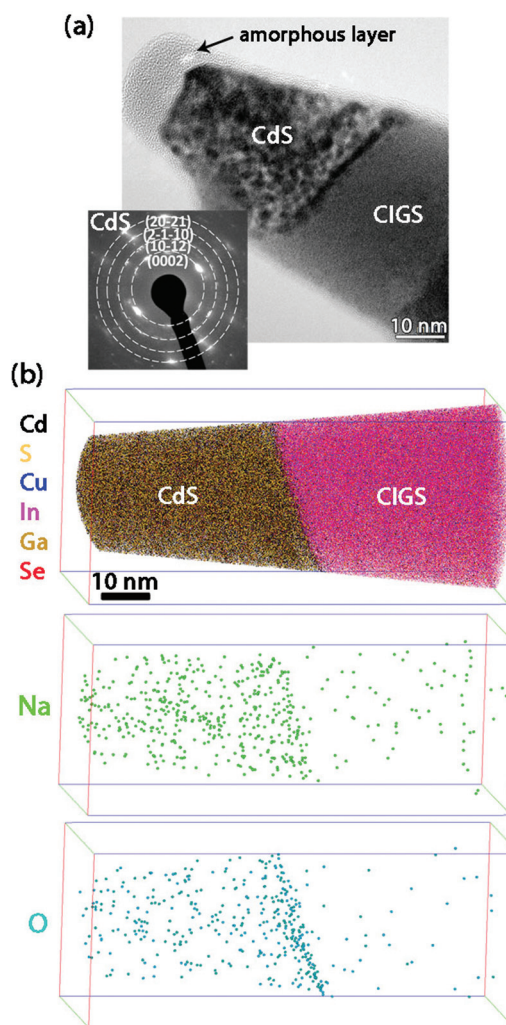


FIG. 2. (a) TEM image of the CdS/CIGS interface in an APT tip before performing final 5 keV milling. Inset shows the diffraction pattern of the CdS layer. (b) APT elemental maps of Cu (blue), In (pink), Ga (orange), Se (red), Cd (black), S (yellow), Na (green), and O (light blue). Volume size is $36 \times 36 \times 85 \text{ nm}^3$.

single stage CIS solar cells,¹⁰ we propose that Cu vacancies within the first 2–3 atomic monolayers of the CIGS surface may be occupied by Cd atoms, forming Cd_{Cu}^+ donor defects. This scenario is likely due to the similar ionic radii of Cd^{2+} (0.097 nm) and Cu^+ (0.096 nm) ions.⁵ The ionic radius of Ga^{3+} is reported to be only 0.062 nm. Thus, the occupation of vacant Ga-sites to form Cd_{Ga}^- acceptor defects does not appear to be favorable in terms of elastic strain. For a complete understanding of Cd-related point defects in CIGS, first-principles calculations are needed.

The Cu depletion at the CI(G)S surface may be ascribed to the formation of a Cu depleted surface during CI(G)S deposition, so-called surface reconstruction,^{19–21} or/and also to Cu dissolution in the chemical bath during the CdS deposition.⁷ Furthermore, our current and previous APT data¹⁰ do not show the existence of an ordered vacancy compound (OVC- $\text{Cu}(\text{In,Ga})_3\text{Se}_5$), as proposed by Schmid *et al.*,²² at least for the evaluated datasets.

The average CdS composition determined from the concentration profiles exhibits a slight deviation from the nominal 50:50 stoichiometry (see Fig. 3). This is due to overlapping mass-to-charge peaks, namely, $^{113}\text{Cd}^+$ and

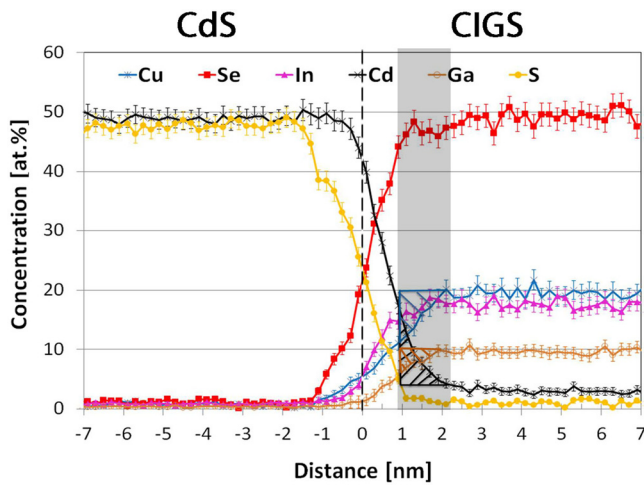


FIG. 3. Proximity histogram across the CdS/CIGS interface, defined by an iso-concentration threshold value of 7 at. % In.

$^{113}\text{In}^+$, $^{140,142,147}\text{CdS}^+$ and $^{140,142,147}\text{CuSe}^+$, which cannot be deconvoluted in the composition profile and lead to an overestimation of the In, Cu, and Se concentration in CdS. To determine a more accurate value for the actual composition of the CdS layer, its mass spectrum was evaluated separately. Overlapping mass peaks were deconvoluted by taking into account the isotope abundances. The values corrected by this procedure are shown for both CdS and CIGS in Table I. The detected average composition of CdS is close to the nominal 50:50 stoichiometry, whereas a very low content of Se and no Cu, In, or Ga was detected in the CdS phase.

The 3D map in Fig. 2(b) shows that O is enriched at the CdS/CIGS_{GB} interface (0.8 ± 0.2 at. % for O), whereas the Na enrichment is not so prominent in the 3D map. Nevertheless from 1D concentration profile (not shown here), we could detect a slight Na enrichment (0.3 ± 0.1 at. %). Furthermore, we detected higher impurity contents in CdS than in CIGS bulk (see Table II). We may assume that Na and O are segregated at the CIGS surface during the CIGS deposition at $\sim 600^\circ\text{C}$ and successively diluted in the CBD solution to be finally redeposited with the CdS layer. Our results are in good agreement with the data of Heske *et al.*,²³ who detected Na enrichment at the CdS/CIGS interface by x-ray emission spectroscopy (XES). Also, our previous studies on single stage CIS solar cells showed similar distributions of Na and O at the CdS/CIS interface.²⁴ One might speculate that the Na and O impurities in the CdS layer could change the electrical properties of the CdS layer, as it is the case for CIGS and CIS, and thereby improve the device performance.

Fig. 4(a) shows the 3D atom maps including the CdS/CIGS_{GB} interface. The interface was oriented nearly parallel

TABLE II. Na and O concentrations in CdS and CIGS bulk for both APT measurements (APT-1 (shown in Fig. 2) and APT-2 (shown in Fig. 4)).

Layer	APT-1 (Fig. 2)		APT-2 (Fig. 4)		
	CdS	CIGS _{bulk}	CdS	CIGS _{bulk}	GB
Na (at. %)	0.09 ± 0.01	0.03 ± 0.01	1.8 ± 0.1	0.013 ± 0.002	6.8 ± 0.7
O (at. %)	0.04 ± 0.01	...	0.15 ± 0.02	0.03 ± 0.003	1.2 ± 0.3

to the tip axis to probe a larger area of the CdS/CIGS interface than in Fig. 2. As specified before, a thin Cu-depleted and Cd-enriched CIGS surface layer was observed (not shown here). The CdS and CIGS compositions determined by deconvolution of overlapping peaks are shown in Table I (see APT-2), where the composition values for CdS and CIGS are similar to those determined in APT-1.

Fig. 4(a) also reveals a GB in the CIGS layer, which is nearly perpendicular to the CdS/CIGS interface and enriched with Cd, Na, and O. This result shows that the GBs in the CIGS layer serve as fast diffusion paths for solutes/impurities, i.e., for diffusion of Cd into CIGS as well as for diffusion of Na and O from the soda-lime glass substrate into CIGS and to its surface. Although the deposition of the CdS layer occurs at very low temperature (typical temperature of CBD solution is $\sim 65^\circ\text{C}$), Cd diffusion along CIGS GBs obviously takes place. The high diffusivity of Cd along CIGS GBs is an indication for a high concentration of Cu vacancies at the GBs.

Fig. 4(b) shows that Na is strongly enriched in the region close to the CdS/CIGS_{GB} interface, whereas O is only slightly enriched at this interface. The high Na-concentration at the CdS/CIGS_{GB} interface ($\sim 10 \pm 1$ at. % Na, compared with O which is only 0.8 ± 0.3 at. %) is due to the presence of Na rich-clusters in this area. These clusters contain in average 10 at. % of Na (the Na concentration inside the clusters varies between 6 ± 0.5 and 22 ± 2 at. %) with ~ 150 atoms/cluster, taking into account the detection efficiency of the APT system used in this work ($\sim 38\%$). The 3D atom map shown in Fig. 4 does not give any conclusion whether the Na clusters are located in the bulk or at the GBs of the nanocrystalline CdS layer.

APT gives accurate quantitative data on the number of Cu atoms replaced by Cd at the CIGS surface over the first ~ 3 atomic monolayers at the CIGS surface. In this area, the Cd density ($\sim 10^{22}\text{ cm}^{-3}$) is substantially larger than the typical hole density in solar-grade CIGS films (10^{15} cm^{-3} – 10^{17} cm^{-3}).²⁵ The composition profile across the CdS/CIGS interface is similar to that previously reported for the CdS/CIS interface in a CIS solar cell.¹⁰ It should be noted that the previously studied CIS thin-film was prepared by an inline

TABLE I. Chemical composition values of CdS and CIGS bulk obtained from APT mass-to-charge spectra after decomposition of overlapping mass peaks.

Analysis	Layer	Cu (at. %)	In (at. %)	Ga (at. %)	Se (at. %)	Cd (at. %)	S (at. %)
APT-1 (Fig. 2)	CdS	0.1 ± 0.01	50.1 ± 0.2	49.5 ± 0.2
	CIGS	22.5 ± 0.2	18.8 ± 0.2	9.5 ± 0.1	49.1 ± 0.3
APT-2 (Fig. 4)	CdS	0.5 ± 0.04	49.8 ± 0.3	47.30 ± 0.3
	CIGS	22.0 ± 0.1	21.7 ± 0.1	7.1 ± 0.03	49.2 ± 0.1

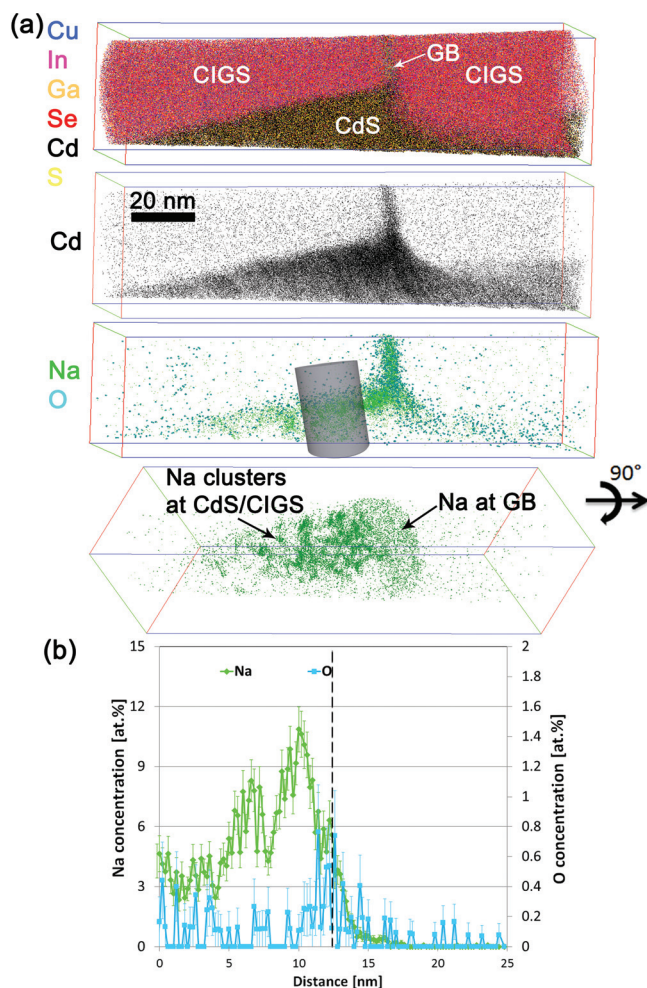


FIG. 4. (a) APT elemental maps of Cu (blue), In (pink), Ga (orange), Se (red), Cd (black), S (yellow), Na (green), and O (light blue). The Na map, rotated 90° with respect to the other maps, clearly shows the presence of Na clusters at the CdS/CIGS interface. Volume size: $42 \times 42 \times 143 \text{ nm}^3$. (b) 1D-concentration profiles of Na (green) and O (light blue) across the CdS/CIGS interface obtained from the cylindrical region of interest in Fig. 4(a).

single stage process,¹³ while the present CIGS thin-film was prepared by a multi-stage inline process,¹² hence with an entirely different growth recipe and absorber composition. Nevertheless, similar Cu and Cd trends across the CdS/CIGS interface are measured.

Several models have been proposed in the literature for the p-n junction in CI(G)S solar cells. While most of these authors assume that the CI(G)S surface is Cu depleted,^{19–21} only a few of them take into account the Cd-doping of the CI(G)S surface.^{7,8,17,26} Nakada¹⁷ found that Cd diffuses 10 nm into the absorber layer and causes a buried homojunction, whereas Liao and Rockett⁸ suggested that Cd is found only in the first 1–3 atomic layers of a CIS thin-layer. Our present and previous¹⁰ results support the findings of Liao and Rockett.⁸ The authors explained the beneficial effect of a high amount of positive charge in the type inverted surface region (Cd_{Cu}^+ -doping of the CI(G)S surface) by the fact that the Fermi level is pinned at the interface close to the conduction band. This configuration is very stable and reduces the recombination activity at the CdS/CI(G)S interface. However, the presence of buried homojunction regions cannot be completely excluded, as previous reports showed that open pores

in the absorber layer can be infiltrated and filled with CdS during CBD.^{7,10}

In the present work, we have also shown that Na and O atoms, originating from the SLG substrate, are segregated at the CdS/CIGS interface. As these impurities are expected to change the electronic band structure, their effects on the charge separation and recombination mechanisms at the p-n junction remain to be studied.

The main experimental findings of our APT studies on the CdS/CIGS interface can be summarized as follows:

- First, a Cu- and Ga-depleted as well as Cd-doped region were detected at the CIGS side of the interface.
- Second, Cd is found to be enriched not only at the CIGS side of the interface but also at the CIGS GBs connected to the CdS layer. With respect to the existing models, the Cd diffusion inside the CIGS grain and in the CIGS GBs may prove the existence of a zone within the CIGS absorber layer which is inverted from p- to n-type.
- Third, Na and O impurities are found to decorate the CdS/CIGS interface, where Na-enriched clusters are detected in the areas close to CIGS GBs.

The authors would like to thank Mr. Wolfgang Dittus and Mr. Stefan Paetel for the CIGS layer preparation and Mr. Axel Eicke for the XRF measurements. Also, the authors would like to thank Dr. Daniel Abou-Ras from HZB Berlin for fruitful discussions. This work was funded by the German Research Foundation (DFG) (Contract No. CH 943/2-1).

¹B. J. Stanbery, *Crit. Rev. Solid State Mater. Sci.* **27**, 73 (2002).

²M. Kemell, M. Ritala, and M. Leskelä, *Crit. Rev. Solid State Mater. Sci.* **30**, 1 (2005).

³L. L. Kazmerski, *J. Electron Spectrosc. Relat. Phenom.* **150**, 105 (2006).

⁴P. Jackson, M. Powalla, E. Lotter, D. Hariskos, S. Paetel, R. Wuerz, R. Menner, and W. Wischmann, *Prog. Photovoltaics* **19**, 894 (2011).

⁵T. Nakada and A. Kunioka, *Appl. Phys. Lett.* **74**, 2444 (1999).

⁶D. Abou-Ras, G. Korstorf, A. Romeo, D. Rudmann, and A. N. Tiwari, *Thin Solid Films* **480–481**, 118–123 (2005).

⁷C. Lei, M. Duch, I. M. Robertson, and A. Rockett, *J. Appl. Phys.* **108**, 114908 (2010).

⁸D. Liao, and A. Rockett, *J. Appl. Phys.* **93**, 9380 (2003).

⁹C. S. Jiang, F. S. Hasoon, H. R. Moutinho, H. A. Al-Thani, M. J. Romero, and M. M. Al-Jassim, *Appl. Phys. Lett.* **82**, 127 (2003).

¹⁰O. Cojocaru-Mirédin, P. Choi, R. Wuerz, and D. Raabe, *Appl. Phys. Lett.* **98**, 103504 (2011).

¹¹B. Gault, F. Vurpillot, A. Vella, M. Gilbert, A. Menand, D. Blavette, and B. Deconihout, *Rev. Sci. Instrum.* **77**, 043705 (2006).

¹²G. Voorwinden, P. Jackson, and R. Kniese, in *Proceedings of the 22nd European Photovoltaic Solar Energy Conference*, Milan, Italy (2007), pp. 2115–2118.

¹³M. Powalla, G. Voorwinden, and B. Dimmler, in *Proceedings of the 14th European Photovoltaic Solar Energy Conference*, Barcelona, Spain, 30 June–4 July, edited by H. A. Ossentbrink, P. Helm, and H. Ehmman (1997), p. 1270.

¹⁴R. Wuerz, A. Eicke, F. Kessler, S. Paetel, S. Efimenko, and C. Schlegel, *Sol. Energy Mater. Sol. Cells* **100**, 132 (2012).

¹⁵K. Thompson, D. Lawrence, D. J. Larson, J. D. Olson, T. F. Kelly, and B. Gorman, *Ultramicroscopy* **107**, 131 (2007).

¹⁶O. C. Hellman, J. A. Vandenbroucke, J. Rüsing, D. Isheim, and D. N. Seidman, *Microsc. Microanal.* **6**, 437 (2000).

¹⁷T. Nakada, *Thin Solid Films* **361–362**, 346–352 (2000).

¹⁸F. Vurpillot, D. Larson, and A. Cerezo, *Surf. Interface Anal.* **36**, 552–558 (2004).

¹⁹H. Mönig, Ch. -H. Fischer, R. Caballero, C. A. Kaufmann, N. Allsop, M. Gorgoi, R. Klenk, H.-W. Schock, S. Lehmann, M. C. Lux-Steiner, I. Lauermann, *Acta Mater.* **57**, 3645–3651 (2009).

²⁰S. B. Zhang and S. H. Wei, *Phys. Rev. B* **65**, 081402 (2002).

- ²¹J. E. Jaffe and A. Zunger, [Phys. Rev. B](#) **64**, 241304 (2001).
- ²²D. Schmid, M. Ruckh, F. Grunwald, and H. W. Schock, [J. Appl. Phys.](#) **73**, 2902 (1993).
- ²³C. Heske, D. Eich, R. Fink, E. Umbach, S. Kakar, T. van Buuren, C. Bostedt, L. J. Terminello, M. M. Grush, T. A. Callcott, F. J. Himpsel, D. L. Ederer, R. C. C. Perera, W. Riedl, and F. Karg, [Appl. Phys. Lett.](#) **75**, 2082 (1999).
- ²⁴P. Choi, O. Cojocaru-Mirédin, and R. Wuerz, “Compositional gradients and impurity distributions in CuInSe₂ thin-film solar cells studied by atom probe tomography,” [Surf. Interface Anal.](#) (in press).
- ²⁵T. Eisenbarth, T. Unold, R. Caballero, C. A. Kaufmann, and H. W. Schock, [J. Appl. Phys.](#) **107**, 034509 (2010).
- ²⁶K. Ramanathan, R. Noufi, J. Granata, J. Webb, and J. Keane, [Sol. Energy Mater. Sol. Cells](#) **55**, 15–22 (1998).